Available online at www.sciencedirect.com
SCIENCE DIRECT®
International Journal of Solids and Structures 42 (2005) 621–636
INTERNATIONAL JOURNAL OF SOLIDS and STRUCTURES
www.elsevier.com/locate/ijsolstr

Numerical simulation of solid state sintering

Michael Braginsky [a,*], Veena Tikare [a], Eugene Olevsky [b]

[a] *Sandia National Laboratories, Department of Materials and Process Modeling, Albuquerque, NM 87185-1411, USA*
[b] *San Diego State University, San Diego, CA, USA*

Received 15 October 2003; received in revised form 15 March 2004
Available online 6 August 2004

Abstract

This paper discusses in detail the development of a numerical model capable of simulating microstructural evolution and macroscopic deformation during sintering of complex powder compacts. The model based on the kinetic Monte Carlo (Potts) approach simulates grain growth, vacancy diffusion, and pore annihilation at grain boundaries, which is responsible for densification. Results of 2D simulations for perfect close-packed and random starting configurations are presented and discussed. The microstructural evolution is used to obtain the sintering stress—the macroscopic stress that is equivalent to the microstructural driving force for deformation.

1. Introduction

Sintering is the processing technique in which parts formed of powder materials are thermally treated at temperatures below the melting point of the main constituent for the purpose of increasing the strength of the parts by bonding particles together. All ceramic materials and many high temperature metals are sintered because this process allows parts to be formed at temperatures well below their melting point, which range from 1400 to 3000 °C depending on the material. A powder compact before sintering is a porous packing of loose powder that is held together by weak surface bonds. Initial porosity of the compact typically ranges from 35% to 50% of full density. During sintering the individual particles fuse together to create a dense, strong monolithic part.

The driving force for the sintering process is the reduction in surface free energy of the particle. This reduction is achieved by diffusional transport of material from the centers of particles to the

* Corresponding author. Tel.: +1 505 284 6766; fax: +1 505 844 9781.
E-mail address: mvbragi@sandia.gov (M. Braginsky).

0020-7683/$ - see front matter © 2004 Elsevier Ltd. All rights reserved.
doi:10.1016/j.ijsolstr.2004.06.022

particle–particle necks. As individual particles fuse, the surface area of the particles decreases. This leads to the free energy reduction in the system, which drives sintering. Macroscopically this driving force can be conceptualized as *sintering stress* (Ashby, 1990; Beere, 1975; Bordia and Scherer, 1988; DeJonghe and Rahaman, 1988; Geguzin, 1984; Rahaman et al., 1986; Skorohod, 1972). Thus, unlike classic mechanical problems where microstructure controls the response of material to some applied load and develops due to the applied load, in sintering, like in many other problems in Materials Science (e.g., recrystallization), microstructural evolution provides the driving force of the deformation. Therefore, accurate simulation of microstructural evolution—the evolution of particle size, shape, and packing, the evolution of pore size, shape, and distribution, details of material transport, etc.—during sintering is necessary to predict macroscopic forces and deformation of a part being sintered.

Similar to other areas of Materials Science, modeling of sintering comprises two distinct approaches: microstructural mesoscopic models and macroscopic continuum models. Despite the significant progress achieved in understanding microstructural processes of sintering, the connection between the micro- and macrostructural models is still approximated by phenomenological constitutive relations based on highly idealized geometries. The latter statement is true not just for the current state of sintering modeling, but also for the state of simulation of a wide range of different phenomena for which macrostructural evolution is determined, at least in part, by microstructural rearrangements. The problem is that macroscopic behavior, while dependent on the underlying local interaction mechanisms, is controlled by the whole set of local interactions, i.e., by collective microstructural phenomena.

Until recently, simulation of microstructural evolution of large systems was not feasible due to the computer power limitations. It is becoming increasingly possible to simulate microstructural behavior of large systems, and this development is paving the way for embedding microstructural evolution into macroscopic models. For instance, in dislocation-based plasticity modeling only in the late 1990s did it become viable to directly calculate interactions of large numbers of dislocations (Schwarz, 1999; Needleman and Van Der Giessen, 2001; Devincre et al., 2001), which in turn allowed plasticity models to move beyond continuum phenomenological theories that rely on field quantities to approximate collective microstructural phenomena (Walgraef and Aifantis, 1988; Kubin and Estrin, 1990; Ananthakrishna, 1993; Glazov and Laird, 1995).

In the modeling of sintering the need for the incorporation of mesoscopic simulations into macroscopic models is even greater because microstructural evolution provides the driving force for macroscopic deformation in sintering. Therefore, a mesoscopic model of sintering capable of simulating large powder compacts could be a step to more realistic macroscopic models. The need for such a model can hardly be overstated. Although great progress has been made in the last 50 years in understanding microstructural evolution during sintering, current models of sintering (Zeng et al., 1998; Pan et al., 1998; Zhou and Derby, 1998; Jagota and Dawson, 1988; Bullard, 1997; Zhang and Scheibel, 1995), still consider highly idealized geometries with limited number of circular or spherical particles. While these models have provided much insight into the sintering process by predicting shrinkage rates, geometric changes in the particles and other information, their ability to predict characteristics of a complex powder compact has remained limited. We present a model that is capable of simulating coarsening and densification in a powder compact at all stages of sintering. This capability will allow us to predict density distribution and macroscopic shape changes in a body.

There is a large body of work treating complex diffusion and transport mechanisms during different stages of sintering (Kuczynski, 1950; Kingery and Berg, 1955; Coble, 1958; Johnson, 1969; Ashby, 1974), usually applied to a rather limited number of particles or particular geometries. For instance, Ashby (Ashby, 1990) assumes sintering of a powder compact consisting of spherical particles of single size and uses statistical methods (Ashby, 1990; Arzt, 1982; Fischmeister et al., 1978; Fischmeister and Arzt, 1983) to determine the number of contact neighbors, sintering pressure, and densification. More recent analytical and numerical models of sintering make fewer assumptions and are able to treat the details of shape change, shrinkage rate or other characteristic more accurately in a sintering compact. These works lead to greater

understanding of the sintering process and to better predictive models of sintering. However, they do not capture the complexity of a real sintering system. Furthermore, these models treat each stage of sintering based on a different set of assumptions, while it would be beneficial to have a unified model capable of treating all the stages of sintering based on the underlying physics.

The model used to simulate sintering in this work is based on the kinetic Monte Carlo (Potts) model (Wu, 1982), which was used successfully to model grain growth and pore migration previously (Anderson et al., 1984; Wejchert et al., 1986; Holm et al., 1991). Hassold et al. (1990) used a similar kinetic Monte Carlo model to simulate final stage sintering, by resizing the pores based on the mean distance between pores. Rather than shrink pores, as Hassold et al. (1990) did, we simulate the formation, diffusion, and annihilation of vacancies. A vacancy annihilation mechanism based on the view developed in the stereological theory of sintering (DeHoff, 1989) is added to the model in order to simulate densification. This mechanism comprises vacancy migration from the pores to grain boundaries and vacancy annihilation at the boundaries. The annihilation occurs at a uniform rate along the grain boundary and yields densification. Centers of mass of adjacent grains move closer together in the process. The methodology was applied to sintering of three particles in a previous work (Tikare et al., 2003). In this work we extend this model to simulate sintering in a complex powder compact consisting of a large number of particles of arbitrary shape. All simulation results presented in this paper are obtained in 2D.

The last part of the paper is devoted to the thermodynamic connection between the mesoscale simulations and macroscopic continuum models of sintering. We discuss a methodology of obtaining the sintering stress from mesoscopic simulations and compare the results with several analytical formulae.

2. Potts model

A kinetic Monte Carlo model (Wu, 1982) was used to simulate 2D microstructural evolution during sintering. It can model the following processes:

1. Grain growth by short range diffusion of atoms from one side of the grain boundary to the other;
2. Long range diffusion of pores by surface diffusion and of vacancies/material by grain boundary diffusion;
3. Vacancy annihilation at grain boundaries. [1]

In the model, an ensemble of grain sites and pore sites is allowed to populate a square lattice. The grain sites can assume one of Q distinct, degenerate states, where the individual state is designated by the symbol q; $q_{\text{grain}} = [1, 2, \ldots, Q]$. The pore sites can assume only one state, $q_{\text{pore}} = -1$. Contiguous grain sites of the same state q form a grain and contiguous pore sites form a pore. Grain boundaries exist between neighboring grain sites of different states, q, and pore-grain interfaces exist between neighboring pore and grain sites. The equation of state for these simulations is the sum of all the neighbor interaction energies in the system given by

$$E = \frac{1}{2}\sum_{i=1}^{N}\sum_{j=1}^{8}(1 - \delta(q_i, q_j)) \tag{1}$$

where N is the total number of sites, $\delta(q_i, q_j)$ is the Kronecker delta with $\delta(q_i = q_j) = 1$ and $\delta(q_i \neq q_j) = 0$, q_i is the state of the grain or pore at site i, and q_j is the state of the nearest neighbor at site j. Thus, the only energy considered in the simulation is the interfacial energy with each unlike neighbor contributing one arbitrary unit of energy to the system. As pore sites can assume only one state, $q_{\text{pore}} = -1$, there are no

[1] In this approximation we refer to a single pore site as a vacancy, while denoting more than one contiguous pore sites as a pore.

pore boundaries and all pores sites coalesce. In contrast, grain sites can assume many different states making grain boundaries possible. This yields a two-component, two-phase system with uniform, isotropic interfacial energies between grains and between grains and pores.

Grain growth is simulated using the method developed in previous works (Anderson et al., 1984; Wejchert et al., 1986; Holm et al., 1991). First a grain site is chosen at random from the simulation space. Then a new state q is chosen at random from the Q possible states in the system. The grain site is temporarily assigned the new state and the change in energy is evaluated using (1). Next the standard Metropolis algorithm is used to perform the grain growth step based on Boltzmann statistics. A random number, R, between 0 and 1 is generated. The transition probability, P, is calculated using

$$P = \begin{cases} \exp\left(\dfrac{-\Delta E}{k_B T}\right) & \text{for } \Delta E > 0 \\ 1 \quad \text{for } \Delta E \leqslant 0 \end{cases} \tag{2}$$

where k_B is the Boltzmann constant and T is temperature. If the $R \leqslant P$, then the grain growth step is accepted, if not, the original state is restored. The simulation temperature used for grain growth was $k_B T = 0$, which has been shown to simulate grain growth well (Holm et al., 1991; Tikare and Cawley, 1998).

Pore migration is simulated using conserved dynamics (Hassold et al., 1990), so that the total number of pore sites and grain sites is the same after a pore migration step. A pore site is chosen and next a neighboring grain site is chosen. The two sites are temporarily exchanged with the grain site assuming a new state q where q results in the minimum energy. This minimum-energy, pore-grain exchange simulates pore migration by surface diffusion (Tikare et al., 2003). The change in energy for this exchange is calculated using (1) and again the standard Metropolis algorithm is used to perform the pore migration step using (2) to determine the transition probability. The simulation temperature used for the pore migration step was $k_B T = 0.7$. This higher temperature was necessary to simulate pore migration and is discussed in another work (Tikare and Holm, 1998). Time in the Potts model is measured in units of Monte Carlo steps (MCS); 1 MCS corresponds to N attempted changes where N is the total number of sites in the system.

Vacancy, for the purposes of this work, is defined as a single pore site surrounded by grain sites. Vacancy annihilation was simulated in the previous work, sintering of three particles, by exchanging the vacancy with a grain site. The grain site for this annihilation event was selected by drawing a straight line from the isolated pore site through the center of mass of the adjacent grain to the outside boundary of that particle. This algorithm conserves mass globally, moves the center of mass of the adjacent grain towards the annihilation site, and annihilates a vacancy. Extending this algorithm to a large system with many particles is not trivial as very few grains have an external surface. The development of the annihilation algorithm will be presented in the following section.

3. Model development for microstructural evolution with densification

Our model incorporates the concept of densification developed in the stereological theory of sintering (DeHoff, 1989). In this approach, the densification mechanism comprises vacancy migration from pores to grain boundaries and vacancy annihilation at the grain boundaries. DeHoff visualized this process as vacancies being painted on the grain boundary, with an entire monolayer of vacancies annihilated, so that the centers of mass of adjacent grains move towards that grain boundary. The rate of the process is limited by the time needed for vacancies to diffuse and cover the entire grain boundary. This process is simulated as follows. A pore site is chosen and, if it happens to be an isolated pore site—a vacancy [2]—in contact with a

[2] In the following we refer to contiguous collections of pore sites as pores, while the term "vacancy" is used to denote single pore sites.

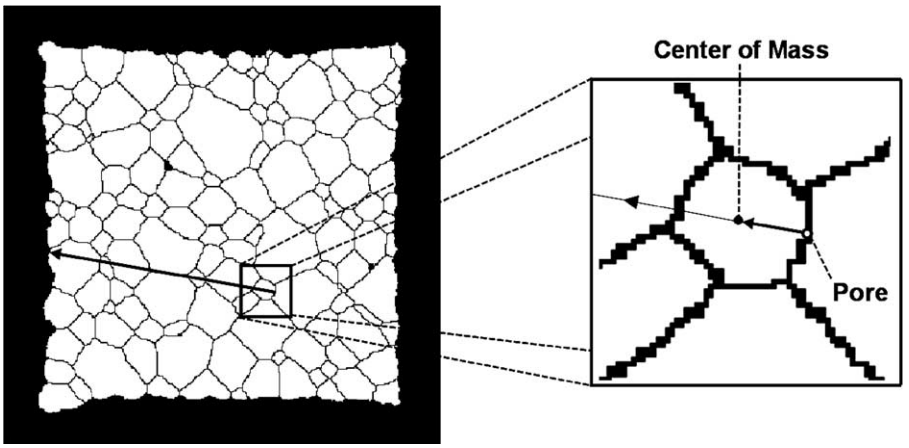

Fig. 1. Schematic of the jump algorithm. Black color denotes pores and grain boundaries; white denotes grains.

grain boundary, it is annihilated. We examined several different algorithms for simulating annihilation. All the algorithms were required to conserve mass globally and to move the centers of mass of the grains adjacent to the site being annihilated closer together. The frequency of annihilation attempts is adjusted inversely proportionally to the average length of grain boundaries, as given by

$$t \propto \left(\frac{L_{gb}}{L_0}\right)^2 \tag{3}$$

to simulate uniform annihilation along grain boundaries.

3.1. The densification algorithm

In this algorithm, pore annihilation is simulated by exchanging a vacancy (an isolated pore site) at a grain boundary with a grain site at the surface. The grain site for the exchange is chosen at the intersection of a line, drawn from the isolated pore site through the center of mass of the adjacent grain, and the outside boundary of the sintering compact. After the exchange the grain site assumes the q state of the adjacent grain. With "jumps" to the outer boundaries of the compact being simulated this routine to a great extent homogenizes local deformation. The schematic of this algorithm is shown in Fig. 1.

For this algorithm to work there has to be a surface. Thus, periodic boundary conditions cannot be used.

3.2. Examples of microstructural evolution

First we performed simulations with perfect close-packed circular particles as the starting configuration. The resulting microstructures at different times are shown in Fig. 2. The densification curve is shown in Fig. 3. Time, as is customary in such simulations, is measured in Monte Carlo steps.

Microstructures shown in Fig. 2 are qualitatively quite similar to the classic experimental results of Alexander and Balluffi (1957) on sintering of copper wires. As time progresses pores become smaller due to the vacancies diffusing along grain boundaries and their subsequent annihilation, centers of mass of adjacent grains come closer together. Internal grains stay the same size since grain boundaries between them have no curvature. They attain the hexagonal equilibrium shape as is expected. External grains, which cannot become hexagonal, tend to decrease in size to reduce the free surface area and, hence, the energy of the system.

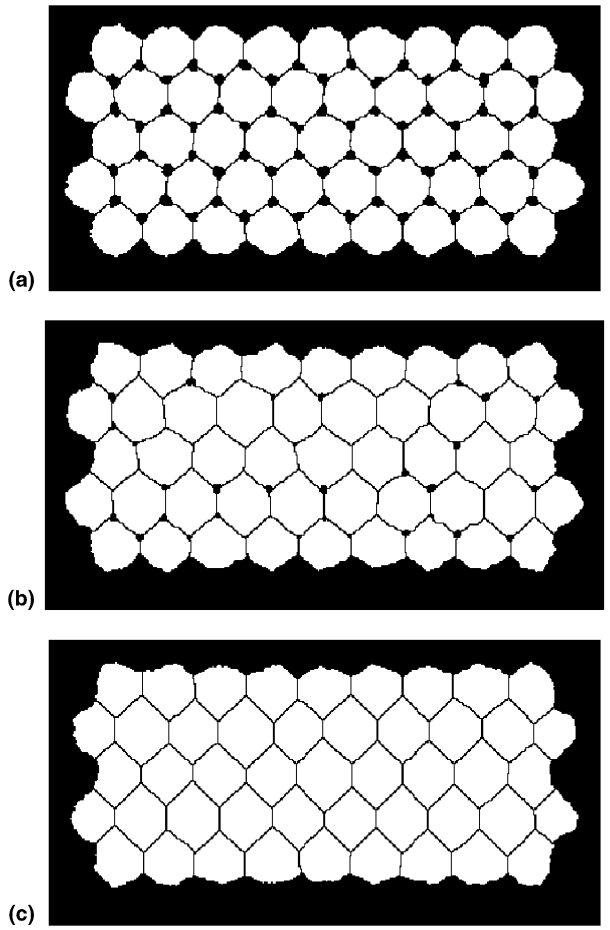

Fig. 2. Microstructures obtained from a perfect close-packed starting configuration: (a) after 10^4 MCS, (b) after 3×10^4 MCS, and (c) after 10^5 MCS.

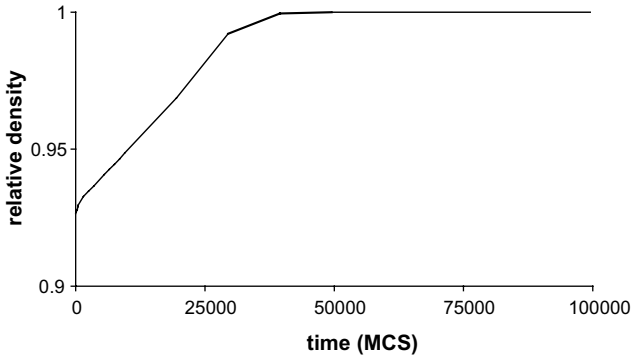

Fig. 3. Densification curve of the close-packed powder compact.

One potential artifact of the model is a possibility of artificial size differences between exterior and interior grains. In order to check whether this occurs, we calculate average sizes of exterior and interior grains. These separate statistics shown in Fig. 4 are needed to understand whether replacing pores with grain sites from the boundary alters the grain size statistics in any significant way. For the close-packed initial configuration these differences are rather small (less than 5%) relative to the average grain size during the simulation. In addition, due to the tendency of outer grains to decrease in size to minimize the energy of the system discussed above, only a part of this difference should be attributed to the possible artifact of the model.

Thus, the algorithm performs well for a perfect close-packed initial configuration and leads to reasonable results.

In order to test the methodology further, we performed calculations with randomly packed equi-axed particles of different sizes and with higher initial porosities. As in the previous simulations vacancies diffuse along the grain boundaries and pores shrink due to annihilations, but, unlike the case of a close-packed initial configuration of same size particles that resulted in straight grain boundaries, systems with a random starting configuration exhibit pore and grain coarsening driven by grain boundaries' curvature. Grain growth accelerates as pores are being annihilated, which suggests, as expected, that grain coarsening is pinned by pores. The densification curve and microstructures at different times are shown in Figs. 5 and 6, respectively.

As stated above, one of our concerns was the possibility that the proposed algorithm alters grain size statistics. Fig. 7 shows grain and pore size statistics for the simulation for a random initial configuration. Here, unlike the case of perfect packing, the difference in grain size of exterior and interior grains is more pronounced, especially, if we consider relative sizes. Nevertheless, grain growth of all grains including exterior grains, as evidenced by Fig. 7, is much higher than the rate of exterior grain shrinkage due to annihilation.

In addition, the number of exterior grains is much smaller than the number of interior grains in these simulations. Therefore, the overall grain statistics is affected only insignificantly.

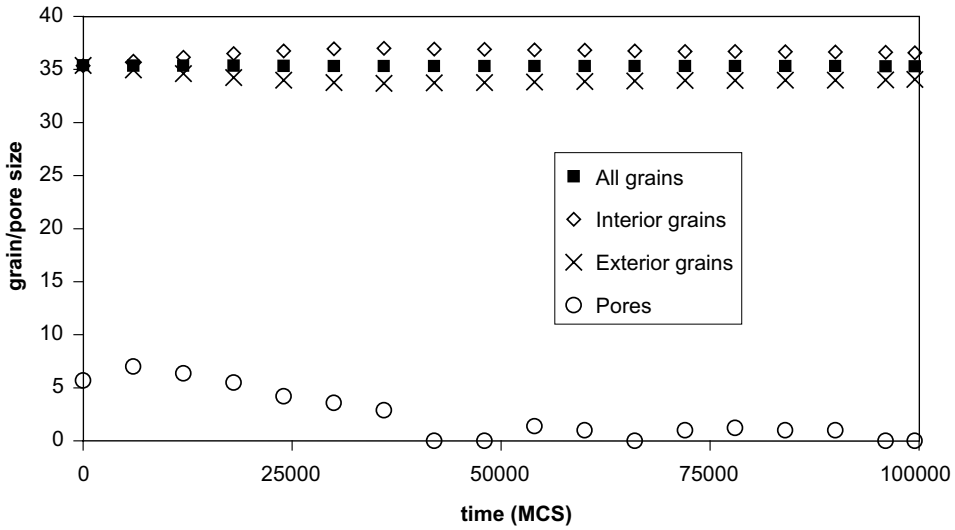

Fig. 4. Grain and pore-size statistics for densification of the close-packed powder compact; Average sizes are shown as function of time (in MCS).

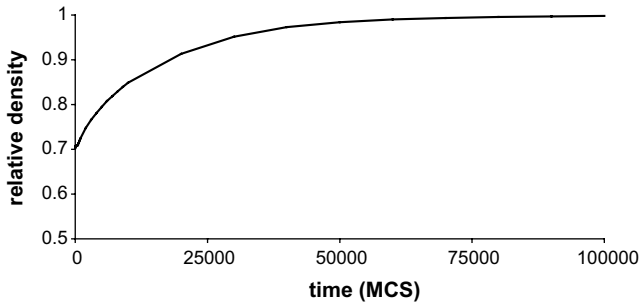

Fig. 5. Densification curve of a randomly packed non-uniform powder.

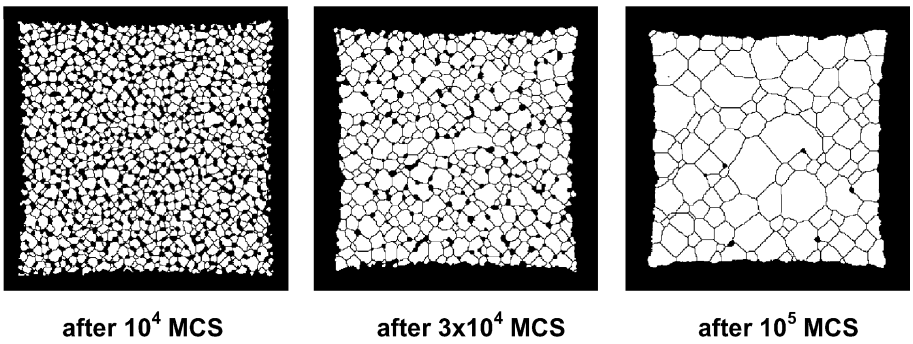

Fig. 6. Microstructural evolution of a randomly packed non-uniform powder.

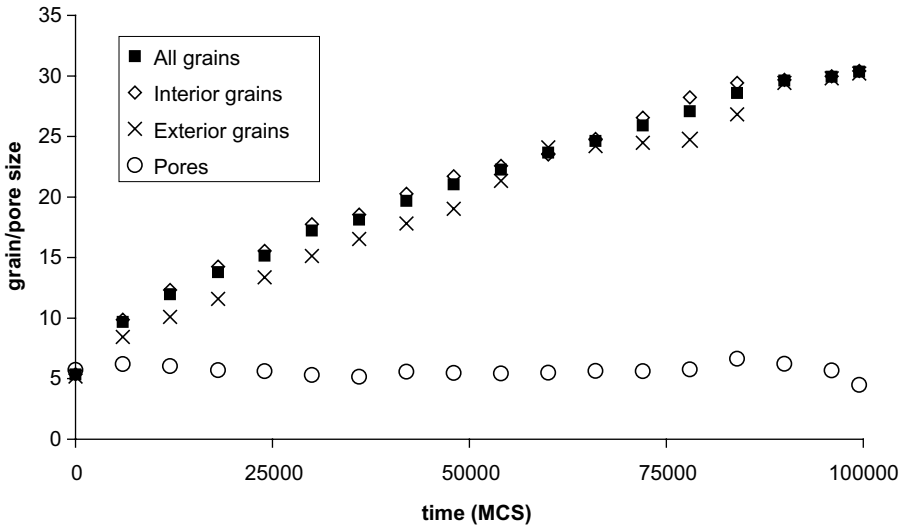

Fig. 7. Grain and pore size statistics for densification of a randomly packed non-uniform powder; average sizes are shown as function of time (in MCS).

4. Sintering stress: connecting microstructural simulations to macroscopic models

In order to simulate sintering, macroscopic continuum models incorporate sintering stress, which is viewed as a macroscopic stress that is equivalent to the microscopic diffusional forces that cause deformation during sintering. The determination of this effective stress and its dependence on microstructural parameters, especially porosity, has been the focus of many works (Ashby, 1990; Beere, 1975; Bordia and Scherer, 1988; DeJonghe and Rahaman, 1988; Rahaman et al., 1986; Skorohod, 1972). Those works rely on derivations that utilize highly idealized geometries.

Having developed the capability to realistically simulate microstructural evolution during sintering, we can use the results of those simulations to calculate the sintering stress for macroscopic constitutive models. In the following analysis such calculations are presented for a viscous model of sintering. The thermodynamic approach is due to Skorohod (1972). [3]

It can be easily shown that if a material is characterized by a free Helmholtz energy that depends on temperature and volume only, the Second Law of thermodynamics can be written as

$$\left(\sigma_{ij} - \rho \frac{\partial H}{\partial V}\delta_{ij}\right) \cdot \dot{\varepsilon}_{ij} \geqslant 0 \tag{4}$$

Here H denotes the Helmholtz free energy, V stands for volume, ρ denotes density, σ_{ij} is the stress tensor, and $\dot{\varepsilon}_{ij}$ is the strain rate. [4] In deriving (4) we used the fact that for viscous materials stress and entropy depend on the strain rate, but not on $dotT$. The system under consideration was also assumed to have no heat flux.

Comparing (4) with the classical thermodynamic requirement for a viscous material

$$\sigma_{ij} \cdot \dot{\varepsilon}_{ij} \geqslant 0 \tag{5}$$

we identify the additional stress term as sintering stress

$$P_{ij} = \rho \frac{\partial H}{\partial V}\delta_{ij} \tag{6}$$

Note that the requirement that the Helmholtz free energy be dependent on the volume leads to a hydrostatic sintering stress.

With this definition, the constitutive equation for a viscous sintering body can be written as

$$\sigma_{ij} = \Lambda_{ij}[\dot{\varepsilon}_{ij}, \theta, \ldots] + P_{ij} \tag{7}$$

where $\Lambda_{ij}[\dot{\varepsilon}_{ij}, \theta, \ldots]$ is a functional defining the constitutive behavior of a viscous material. While such a functional may depend on many microstructural parameters, the dependence on porosity, θ, is necessary for a sintering model.

As stated above, many models have been proposed to obtain the sintering stress based on idealized geometries and microscopic sintering kinetics. The microstructural simulations described in this paper provide a direct method of calculating the sintering stress from (6). Indeed, the microstructural evolution model allows calculation of both volume and free energy as a function of time. Not the entire free energy calculated in the microstructural evolution is related to volume deformation, though. Some microstructural developments, such as grain boundary growth, while reducing the free energy of the system, do not necessarily lead to changes in volume. It is not possible to determine the precise portion of the microstructural

[3] For English-speaking readers a detailed discussion of this approach is given in Olevsky (1998).

[4] While the chosen notation is valid for small strains only, the statement is valid for finite deformations, in which case the strain rate has to be replaced by the symmetric part of the velocity gradient (D). We use the small strain notation here for consistency with Olevsky (1998) to which the reader is referred for details.

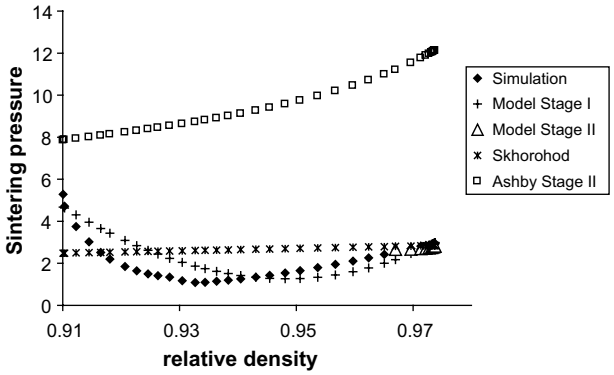

Fig. 8. Sintering stress for the perfect close-packed compact as the function of relative density.

free energy associated with deformation, but the free energy of the pore surfaces is a very good approximation, because it is exactly the reduction of pore surface that drives sintering.

Fig. 8 shows the calculated sintering stress for the closed-packed initial configuration with comparison to the Ashby model (Ashby, 1990) and Skorohod model (Skorohod, 1972). [5] The sintering stress obtained from microstructural simulations is, obviously, quite different from the analytical predictions. That is not surprising, since the analytical models assume geometries that are different from the actual microstructural development. In particular, Skorohod (1972) assumes a statistical distribution of spherical pores, while the Ashby (1990) second stage model assumes closed uniformly distributed spherical pores at the corners of tetradecahedron grains. A close examination of the microstructural simulation for the closed-packed initial configuration reveals that in the process of sintering, the pore undergoes a topological change from concave pores of the initial configuration to the convex pores, which disappear at the end of the process. Moreover, the same development is seen in the classic experiment of Alexander and Balluffi (1957) on sintering of copper wires. [6] In our simulation, we need not make any assumptions about the particle or pore shapes and thus can obtain more accurate sintering stress for different microstructures.

We hypothesized that this topological change is responsible for the form of the sintering stress dependence on density. To test this hypothesis, we developed an analytical model specifically for the closed-packed microstructure with an emphasis on the pore topology. Because of the change in topology the model requires two parts: the initial stage with concave pores and the final stage with convex pores. Assuming the ideal closed-packed structure, we can limit ourselves to the consideration of just one pore.

For the initial stage model consider a pore between three particles in the close-packed structure having nine circular edges (Fig. 9). Three of the edges are the surfaces of the particles, while matter squeezed into the pore by sintering forms the six smaller edges. The schematic with two particles showing the geometric details of this construction is given in Fig. 10. The smaller edges are needed to ensure a 120° angle at the triple junctions. This angle is a natural assumption that follows from the energy balance at a junction.

[5] Two other analytical models for sintering stress that we compared to our results—Bouvard and McMeeking (1996) and Svoboda and Riedel (1992)—are quite close to the Skorohod's model in this case; they are not shown in Fig. 8 to make the picture more readable.

[6] This experiment is the most suitable for comparisons with 2D simulations.

The particles are assumed to stay circular except for the pore boundary and the grain boundaries, which are straight. As particle centers come closer together excess material from the overlapping zones is squeezed into adjacent pores. This causes radii of small edges to increase, which is, essentially, the reason for the decrease in sintering pressure. As the edges grow closer together, they will eventually touch, which happens at a density of around 0.96. The pore then becomes a three edge concave (Fig. 11). The connection between the pore surface, which determines the free energy, and the distance between the centers of the particles is determined based on the requirement of mass conservation—the amount of the material squeezed into the pore has to be equal to the overlapping areas between the particles.

$$\left(\beta - \frac{1}{2}\sin(2\beta)\right)R^2 = \frac{1}{2}d(h-f) - (\alpha-\beta)R^2 - \delta^2(\gamma - \sin(\gamma)) - \frac{1}{2}\delta(2\cos(\alpha)-1)(h-l) \tag{8}$$

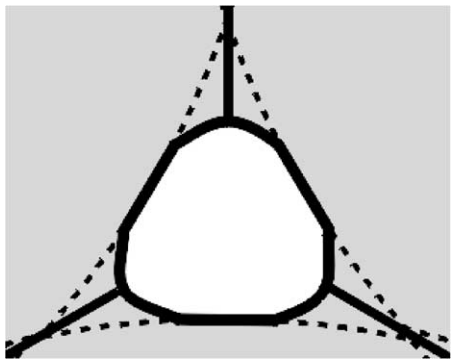

Fig. 9. Schematic of the pore form in the initial sintering for a closed-packed structure. Grey areas belong to grains, solid black lines are the gain and pore surfaces, and the dashed black line shows the initial form of the pore.

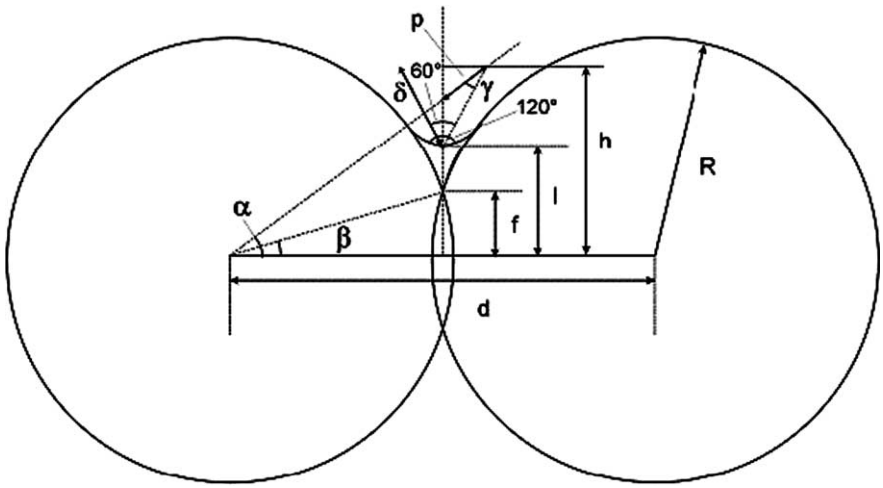

Fig. 10. Geometry of the initial stage of 2D sintering.

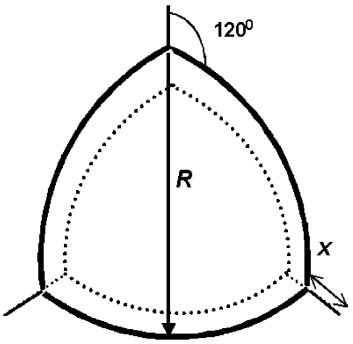

Fig. 11. A three edge concave pore. Straight black segments are grain boundaries, the dotted lines show the self-similar pore evolution.

The notation is given in Fig. 10. In addition, we have geometric connections between different variables

$$\begin{aligned}
\gamma &= \frac{\pi}{3} - \alpha \\
d &= \sqrt{\frac{2\pi}{\rho\sqrt{3}}}R \\
\beta &= \cos^{-1}\left(\frac{d}{2R}\right) \\
\alpha &= \cos^{-1}\left(\frac{d+\delta}{2R}\right) \\
f &= R\sin(\beta) \\
h &= \left(R + \delta - \frac{\delta}{2\cos(\alpha)}\right) \\
l &= (R+\delta)\sin(\alpha) - \delta\cos\left(\frac{\pi}{6}\right)
\end{aligned} \tag{9}$$

here ρ denotes relative density as before.

Unfortunately, the problem does not have an analytical solution, but it can be reduced to a transcendental equation, which can be solved numerically. This was done using the software package Mathematica 3 from Wolfram Research. The numerical results for this sintering stress labeled "Model Stage I" are shown in Fig. 8.

For the concave pore of Fig. 11 (Stage II), the sintering stress can be determined analytically. Indeed, the pore perimeter and the pore area can be easily calculated as

$$\begin{aligned}
L_{\text{pore}} &= \pi R \\
A_{\text{pore}} &= \frac{1}{2}R^2(\pi - \sqrt{3})
\end{aligned} \tag{10}$$

which leads to the sintering pressure being

$$P = \frac{\gamma}{R}\sqrt{\frac{\pi}{\pi - \sqrt{3}}}\sqrt{\frac{\rho}{1-\rho}} \tag{11}$$

This sintering stress is labeled "Model Stage II" in Fig. 8. Notice, that as stated above, the transition to this stage occurs at the relative density about 0.96.

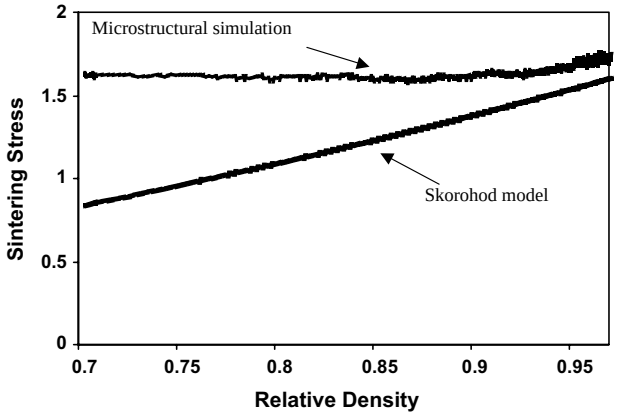

Fig. 12. Sintering stress for the randomly packed non-uniform powder.

As seen from Fig. 8, our model has qualitatively the same behavior as the simulation results, which suggests that, indeed, the sintering pressure is very sensitive to the topological changes in the pore shape. Quantitatively, the analytical model does not coincide with the simulation results because the idealized assumptions—like the one that particles stay circular except for the pore boundary and the grain boundaries, which are straight—are not satisfied exactly in the microstructural simulations. This, once again, underscores the main point that in order to determine sintering stress, one must consider realistic microstructural topologies.

We have determined the sintering stress for the randomly packed non-uniform powder discussed above also. As seen from Fig. 12, it stays nearly constant through the whole simulation. As in the case of the closed-packed compact, the comparison with analytical models—we show the Skorohod model calculation in Fig. 12—is not very good.

5. Discussion and conclusions

A model capable of realistic simulation of the microstructural evolution of a complex powder compact has to satisfy several criteria. First of all, the model should not have any a priori geometric assumptions. Second, the model should not rely on semi-arbitrary division of the sintering process into stages, relying, rather, on more local, basic physical processes. The problem with the stages—and most current sintering models have 2 or 3 stages—is that there are no exact points when one stage ends and the next begins because the distinction between the stages is based on overall or average characteristics of the compact. Consider, for instance, Ashby's model (Ashby, 1990) that distinguishes two stages of sintering (microstructures with open and closed porosity) with different densification laws. Density is used as the criterion for considering the compact in one or the other stage in this model, with the second stage starting at 0.92 of the theoretical density of the compact. This value is based on consideration of a powder compact with spherical particles and, thus, incorporates geometric assumptions. Other models use similar approaches to criteria dividing the process of sintering into stages. And, the final requirement is that the model should be scalable, i.e., it should be able to simulate large powder compacts.

The simulation technique we present satisfies all three requirements. The model does not need any geometric assumptions because the microstructural development is simulated based on a set of simple *local* rules and overall thermodynamic laws. The state of each pixel depends only on the state of its neighboring pixels, not on the state of the whole system at each point in time. Thus, the system can exhibit the open and

closed porosity stages as seen in microstructures in Fig. 6. However, the model does not require any a priori information on those stages or any change in the simulation rules when the porosity becomes closed. The Potts model, which is the basis of our sintering model, has been shown to be scalable (Anderson et al., 1984; Wejchert et al., 1986; Holm et al., 1991). The addition of the annihilation mechanism, understandably, slows the calculation, but not very significantly and does not require more memory usage. Therefore, the third requirement is satisfied also.

The small artifact that the annihilation algorithm introduces—namely, the difference in average grain size between the exterior and interior grains due to the annihilation procedure—is not significant because the rate of grain growth is much higher than the rate of artificial shrinkage of the exterior grains. In addition, being a boundary effect, this artifact becomes less and less important with the increase of the simulation size.

There is another important characteristic of the model that we need to address: by moving porosity to the boundary regions, the procedure homogenizes the deformation of the simulation area. This feature might even be conducive for the connection to macroscopic continuum models, which require some average, or homogenized, information from the microstructures, but because of it the algorithm does not allow for the defect growth that occurs in many materials during sintering. The algorithm does allow for modifications, like jumps to defects in addition to the jumps to the boundary of the compact, which can simulate the defect growth. This issue together with the generalization to 3D, which is usually straightforward for kinetic Monte Carlo algorithms, will be the focus of the further development of the mesoscopic model.

The thermodynamic connection between the microstructural simulations and the macroscopic continuum models of sintering is one of the most important parts of the presented work. The methodology discussed is applicable for the systems with hydrostatic sintering stress, which is the case commonly used. Currently, discussions of anisotropic sintering and, hence, of a possibility of a non-hydrostatic sintering stress start to appear in literature (e.g., Tikare et al., accepted; Raj and Cannon, 1999; Stedman et al., 1993; Watanabe et al., 1989). Our methodology of calculating the sintering stress is not directly applicable to such a case. The reason is that the thermodynamic definition of the sintering stress analogous to (6) would require the calculation of a tensor derivative of the free energy with respect to macroscopic strain, while in the simulation the components of the macroscopic strain are given as functions of time and, hence, are not independent for a simulation run. While the mesoscopic model is readily applicable to the case of anisotropic sintering, as shown by Tikare et al. (accepted), the corresponding case of a non-hydrostatic sintering stress requires additional study.

Acknowledgment

Sandia is a multiprogram laboratory operated by Sandia Corporation, a Lockheed Martin Company, for the United States Department of Energy's National Nuclear Security Administration under the Contract DE-AC04-94AL-85000.

References

Alexander, B.H., Balluffi, R.W., 1957. The Mechanism of Sintering of Copper. Acta Metallurgica et Materialia 5, 666–677.

Ananthakrishna, G., 1993. Formation, propagation of bands and chaos in Jerky flow. Scripta Metallurgica et Materialia 29 (9), 1183–1188.

Anderson, M.P., Srolovitz, D.J., Grest, G.S., Sahni, P.S., 1984. Computer-simulation of grain-growth. 1. Kinetics. Acta Metallurgica et Materialia 32 (5), 783–791.

Arzt, E., 1982. The influence of an increasing particle coordination on the densification of spherical powders. Acta Metallurgica et Materialia 30 (10), 1883–1890.

Ashby, M.F., 1974. First report on sintering diagrams. Acta Metallurgica et Materialia 22 (3), 275–289.
Ashby, M.F., 1990. Background Reading, HIP 6.0. University of Cambridge, Cambridge, UK.
Beere, W., 1975. The second stage sintering kinetics of powder compacts. Acta Metallurgica 23 (1), 139–145.
Bordia, R.K., Scherer, G.W., 1988. On constrained sintering. 2. Comparison of constitutive models. Acta Metallurgica 36 (9), 2399–2409.
Bouvard, D., McMeeking, R.M., 1996. The deformation of interparticle necks by diffusion controlled creep. Journal of the American Ceramic Society 79 (3), 666–672.
Bullard, J.W., 1997. Digital-image-based models of two-dimensional microstructural evolution by surface diffusion and vapor transport. Journal of Applied Physics 81 (1), 159–168.
Coble, R.L., 1958. Initial sintering of alumina and hematite. Journal of the American Ceramic Society 41 (2), 55–62.
DeHoff, R.T., 1989. Stereological theory of sintering. In: Uskokovic, D.P. et al. (Eds.), Science of Sintering. Plenum Press, New York, pp. 55–71.
DeJonghe, L.C., Rahaman, M.N., 1988. Sintering stress of homogeneous and heterogeneous powder compacts. Acta Metallurgica 36 (1), 223–229.
Devincre, B., Kubin, L.P., Lemarchand, C., Madec, R., 2001. Mesoscopic simulations of plastic deformation. Materials Science and Engineering A 309 (SISI), 211–219.
Fischmeister, H.F., Arzt, E., Olsson, L.R., 1978. Particle deformation and sliding during compaction of spherical powders: study by quantitative metallography. Powder Metallurgy 21 (4), 179–187.
Fischmeister, H.F., Arzt, E., 1983. Densification of powders by particle deformation. Powder Metallurgy 26 (2), 82–88.
Geguzin, Y.E., 1984. Physics of sintering, Second ed. Nauka, Moscow (in Russian).
Glazov, M.V., Laird, C., 1995. Size effects of dislocation patterning in fatigued metals. Acta Metallurgica et Materialia 43 (7), 2849–2857.
Hassold, G.N., Chen, I.-W., Srolovitz, D.J., 1990. Computer-simulation of final-stage sintering. 1. Model, kinetics, and microstructure. Journal of the American Ceramic Society 73 (10), 2857–2864.
Holm, E.A., Glazier, J.A., Srolovitz, D.J., Grest, G.S., 1991. Effects of lattice anisotropy and temperature on domain growth in the 2-dimensional Potts-model. Physical Review A 43 (6), 2662–2668.
Jagota, A., Dawson, P.R., 1988. Micromechanical modeling of powder compacts. 1. Unit problems for sintering and traction induced deformation. Acta Metallurgica et Materialia 36 (9), 2551–2561.
Johnson, D.L., 1969. New method of obtaining volume grain-boundary and surface diffusion coefficients from sintering data. Journal of Applied Physics 40 (1), 192.
Kingery, W.D., Berg, M., 1955. Study of the initial stages of sintering solids by viscous flow, evaporation–condensation, and self-diffusion. Journal of Applied Physics 26 (10), 1205–1212.
Kubin, L.P., Estrin, Y., 1990. Evolution of dislocation densities and the critical conditions for the Portevin–Lechatelier effect. Acta Metallurgica et Materialia 38 (5), 697–708.
Kuczynski, G.C., 1950. Measurement of self-diffusion of silver without radioactive tracers. Journal of Applied Physics 21 (7), 632–635.
Needleman, A., Van Der Giessen, E., 2001. Discrete dislocation and continuum descriptions of plastic flow. Materials Science and Engineering A 309 (SISI), 1–13.
Olevsky, E.A., 1998. Theory of sintering: from discrete to continuum. Materials Science and Engineering R 23 (2), 41–100.
Pan, J., Le, H., Kucherenko, S., Yeomans, J.A., 1998. A model for the sintering of spherical particles of different sizes by solid state diffusion. Acta Materialia 46 (13), 4671–4690.
Rahaman, M.N., Brook, R.J., DeJonghe, L.C., 1986. Effect of shear-stress on sintering. Journal of American Ceramic Society 69 (1), 53–58.
Raj, P.M., Cannon, W.R., 1999. Anisotropic shrinkage in tape-cast alumina: role of processing parameters and particle shape. Journal of the American Ceramic Society 82 (10), 2619–2625.
Svoboda, J., Riedel, H., 1992. Pore-boundary interactions and evolution-equations for the porosity and the grain-size during sintering. Acta Metallurgica et Materialia 40 (11), 2829–2840.
Schwarz, K.W., 1999. Simulation of dislocations on the mesoscopic scale: I: methods and examples. Journal of Applied Physics 85 (1), 108–119.
Skorohod, V.V., 1972. Rheological Basis of the Theory of Sintering. Naukova Dumka, Kiev.
Stedman, S.J., Evans, J.R.G., Brook, R.J., Hoffmann, M.J., 1993. Anisotropic sintering shrinkage in injection-moulded composite–ceramics. Journal of the European Ceramic Society 11 (6), 523–532.
Tikare, V., Braginsky, M., Olevsky, E., 2003. Numerical simulation of solid state sintering I: sintering of three particles. Journal of the American Ceramic Society 86 (1), 49–53.
Tikare, V., Cawley, J.D., 1998. Application of the Potts model to simulation of Ostwald ripening. Journal of the American Ceramic Society 81 (3), 485–491.
Tikare, V., Holm, E.A., 1998. Simulation of grain growth and pore migration in a thermal gradient. Journal of the American Ceramic Society 81 (3), 480–484.

Tikare, V., Braginsky, M., Olevsky. E., Johnson, D.L., accepted. Numerical simulation of anisotropic shrinkage in a 2D compact of elongated particles. Accepted by the Journal of the American Ceramic Society.

Walgraef, D., Aifantis, E.C., 1988. Plastic instabilities, dislocation patterns and nonequilibrium phenomena. Res Mechanica 23 (2–3), 161–195.

Watanabe, H., Kimura, T., Yamaguchi, T., 1989. Particle orientation during tape-casting in the fabrication of the grain-oriented bismuth titanate. Journal of the American Ceramic Society 72 (2), 289–293.

Wejchert, J., Weaire, D., Kermode, J.P., 1986. On the distribution of cell areas in a Voronoi network. Philosophical Magazine B-Physics of Condensed Matter 53 (5), L101–L105.

Wu, F.Y., 1982. The Potts-model. Reviews of Modern Physics 54 (1), 235–268.

Zeng, P., Zajac, S., Clapp, P.C., Rifkin, J.A., 1998. Nanoparticle sintering simulations. Materials Science and Engineering A 252 (2), 301–306.

Zhang, W., Scheibel, J.H., 1995. The sintering of 2 particles by surface and grain-boundary diffusion: a 2-dimensional numerical study. Acta Metallurgica et Materialia 43 (12), 4377–4386.

Zhou, H., Derby, J.J., 1998. Three-dimensional finite-element analysis of viscous sintering. Journal of the American Ceramic Society 81 (3), 533–540.